Mixed Amphiphilic Polymeric Nanoparticles of Chitosan, Poly(Vinyl Alcohol) and Poly(Methyl Methacrylate) for Intranasal Drug Delivery: A Preliminary *in Vivo* Study

Inbar Schlachet, Hen Moshe Halamish and Alejandro Sosnik[1,*]

[1] Laboratory of Pharmaceutical Nanomaterials Science, Department of Materials Science and Engineering, Technion-Israel Institute of Technology, Haifa, Israel

[*] Correspondence: Laboratory of Pharmaceutical Nanomaterials Science, De-Jur Bldg., Office 607, Department of Materials Science and Engineering, Technion-Israel Institute of Technology, 3200003 Haifa, Israel; Email: sosnik@technion.ac.il, alesosnik@gmail.com; Tel.: +972-77-887-1971

Abstract: Intranasal (i.n.) administration became an alternative strategy to bypass the blood-brain barrier and improve drug bioavailability in the brain. The main goal of this work was to preliminarily study the biodistribution of mixed amphiphilic mucoadhesive nanoparticles made of chitosan-*g*-poly(methyl methacrylate) and poly(vinyl alcohol)-*g*-poly(methyl methacrylate) and ionotropically crosslinked with sodium tripolyphosphate in the brain after intravenous (i.v.) and i.n. administration to Hsd:ICR mice. After i.v. administration, the highest nanoparticle accumulation was detected in the liver, among other peripheral organs. After i.n. administration of a 10-times smaller nanoparticle dose, the accumulation of the nanoparticles in off-target organs was much lower than after i.v. injection. In particular, the accumulation of the nanoparticles in the liver was 20 times lower than by i.v. When brains were analyzed separately, intravenously administered nanoparticles accumulated mainly in the "top" brain, reaching a maximum after 1h. Conversely, in i.n. administration, nanoparticles were detected in the "bottom" brain and the head (maximum reached after 2 h) owing to their retention in the nasal mucosa and could serve as a reservoir from which the drug is released and transported to the brain over time. Overall results indicate that i.n. nanoparticles reach similar brain bioavailability, though with a 10-fold smaller dose, and accumulate in off-target organs to a more limited extent and only after redistribution through the systemic circulation. At the same time, both administration routes seem to lead to differential accumulation in brain regions and thus, they could be beneficial in the treatment of different medical conditions.

Keywords: Central nervous system (CNS); blood-brain barrier (BBB); self-assembled polymeric nanoparticles; intranasal delivery; biodistribution

1. Introduction

The treatment of diseases of the central nervous system (CNS) by systemic drug administration is challenging owing to the presence of the blood-brain barrier (BBB) and the blood-cerebrospinal fluid barrier [1]. The BBB excludes more than 95% of the small-molecule and biological drugs from crossing into the brain [2,3]. In addition, the BBB displays different efflux transporters that transport substrate molecules (e.g., drugs) out of the brain endothelium, against a concentration gradient [4,5]. Drugs that do not comply with fundamental physicochemical characteristics such as high lipid solubility, low molecular weight and less than 8-10 H bonds with water cannot cross the BBB and their bioavailability and pharmacological efficacy diminished [2].

New delivery approaches that increase drug delivery to the CNS are under intense investigation [6]. The transient disruption of the BBB by osmotic shrinkage of the endothelial cells together with the opening of BBB tight junctions by intracarotid arterial infusion of non-diffusive solutes such as mannitol is one of them [7]. A main drawback is that increased permeability might also enable the passage of plasma proteins and result in abnormal neuronal function [8]. Another strategy is the use of carrier-mediated transport systems that transport nutrients such as glucose and amino acids into the CNS [8]. Drugs with the proper molecular design that not always complies with the structure-activity relationship can be recognized by these influx transporters and show high permeability across the BBB [2,8,9]. Over the last decades, a plethora of nanotechnology strategies have been investigated to overcome the limited ability to deliver active molecules from the systemic circulation into the CNS [10-15]. For this, drug-loaded nanoparticles of different nature (e.g., lipid, polymeric) and size are surface-decorated with ligands that bind receptors overexpressed in the BBB and cross the BBB by transcytosis [16,17].

The existence of a nose-to-brain pathway that bypasses the BBB has been evidenced by the accumulation and harm caused by environmental nanoparticulate matter in the CNS [18-21]. With the emergence of nanomedicine, different types of pure drug nanocrystals and nanoparticles were designed and their CNS bioavailability following intranasal (i.n.) administration assessed [22-26]. Recent studies confirmed the advantage of i.n. administration of nanocarriers over the intravenous (i.v.) route to increase drug bioavailability in the olfactory bulb. Among the different nanotechnology delivery platforms, polymeric micelles are among the most promising [27]. For example, in an early study, we demonstrated that the i.n. administration of the antiretroviral efavirenz nanoencapsulated within core-corona polymeric micelles made of poly(ethylene oxide)-*b*-poly(propylene oxide) (PEO-PPO) block copolymers significantly increases its bioavailability in the brain of rat with respect to the i.v. counterpart [28]. In this context, fundamental nanoparticle features (e.g., size, shape, surface chemistry) that govern the nose-to-brain transport remain to be elucidated [29]. For instance, the size, the shape and/or the surface chemistry and charge could change the transport pathway.

PEO-PPO polymeric micelles show limited encapsulation capacity for many hydrophobic cargos and low physical stability upon dilution over time. In this context, we developed mucoadhesive amphiphilic polymeric nanoparticles produced by the aggregation of chitosan (CS) and poly(vinyl alcohol) (PVA) graft copolymers hydrophobized in the side-chain with different hydrophobic blocks such as poly(methyl methacrylate) (PMMA) and their physical stabilization by non-covalent crosslinking of CS and PVA domains with sodium tripolyphosphate (TPP) and boric acid, respectively [30-32]. These nanoparticles display a multimicellar nanostructure [33,34] and very high physical stability under extreme dilution [30-32]. Aiming to understand the cellular pathways involved in this transport, we recently investigated the interaction of these polymeric nanoparticles with primary olfactory sensory neurons, cortical neurons and microglia isolated from olfactory bulb, olfactory epithelium and cortex of newborn rats [35]. Our results strongly suggested the involvement of microglia (and not cortical or olfactory neurons) in the nose-to-brain transport of nanoparticulate matter.

CS has been extensively investigated as mucoadhesive drug nanocarrier and its cytotoxicity a matter of debate [36,37], including for i.n. drug delivery [38-40]. Most works reported on the good cell compatibility of this polysaccharide that is classified as "generally recognized as safe" (GRAS) by the US Food and Drug Administration (FDA) [41]. However, CS nanoparticles has been associated with cell toxicity because of the electrostatic interaction of the positively-charged surface with the negatively-charged cell membrane and the toxicity level depends on the cell type [42].

Aiming to capitalize on the potential of our versatile amphiphilic nanocarriers in mucosal drug delivery in general and in nose-to-brain administration in particular, we preliminary investigated the cell compatibility of CS-*g*-PMMA nanoparticles in human primary nasal epithelial cells and showed their high toxicity [43]. In this context, we produced mixed CS-*g*-PMMA:PVA-*g*-PMMA (1:1 weight

ratio) nanoparticles that display better human nasal cell compatibility than the CS-based counterparts owing to a decrease of the surface charge density, as expressed by a less positive zeta-potential (Z-potential). In addition, we demonstrated that they cross a model of nasal epithelium *in vitro* [43]. These nanoparticles encapsulated two experimental anti-cancer drugs [44]. In this work, we preliminarily investigated the biodistribution of these mixed amphiphilic nanoparticles after i.n. administration to mice and compared it to the i.v. route for the first time.

2. Results and Discussion

Mixed nanoparticles were produced by the solvent casting method that comprised co-dissolution of identical amounts of CS-PMMA30 (a CS-*g*-PMMA copolymer containing 30% w/w of PMMA) and PVA-PMMA16 (a PVA-*g*-PMMA copolymer containing 16% w/w of PMMA) in dimethyl sulfoxide (DMSO), drying under vacuum and redispersion in water [43,45]. Self-assembly takes place once the critical aggregation concentration (CAC) is surpassed. The CAC of CS-PMMA30 and PVA-PMMA16 is in the 0.04-0.05% w/v range [32-34]. Since the self-assembly process is random, by utilizing this method, we anticipated the formation of mixed nanoparticles with very similar qualitative and quantitative composition. To physically stabilize the nanoparticle, CS domains were crosslinked by the formation of a polyelectrolyte complex with TPP. The size, size distribution and Z-potential of 0.1% w/v non-crosslinked and crosslinked mixed CS-PMMA30:PVA-PMMA16 nanoparticles before the *in vivo* studies were analyzed by dynamic light scattering (DLS), at 25°C [43]. Non-crosslinked and crosslinked nanoparticles showed monomodal size distribution (one size population), while the polydispersity index (PDI), which is a measure of the size distribution, slightly changed after the ionotropic crosslinking; e.g., non-crosslinked mixed CS-PMMA30:PVA-PMMA16 nanoparticles showed a hydrodynamic diameter (D_h) of 193 ± 62 nm and a PDI of 0.23 (**Supplementary Table 1**) [43]. This size is similar to the shown by pure CS-PMM30 (D_h of 184 ± 4 nm; PDI of 0.20) nanoparticles and larger than that of pure PVA-PMMA16 counterparts of the same concentration (D_h of 92 ± 4 nm and PDI of 0.14) [32-34]. Crosslinking of a 0.1% w/v nanoparticle suspension with TPP solution in water (1% w/v; 2.5 μL per mL of nanoparticles) resulted in an increase of the size to 249 ± 26 nm and of the PDI to 0.26, and their full physical stabilization [43]. Pure crosslinked CS-PMM30 nanoparticles are larger 332 ± 54 nm (PDI of 0.33) owing to nanoparticle bridging [32], a phenomenon that is less likely in mixed particles that contain 50% w/w of non-ionic PVA-PPMA16, a copolymer that does not interact with TPP.

The surface charge of nanoparticulate matter affects their cell compatibility and usually, positively-charged particles are more cytotoxic than neutral and negatively-charged ones [46]. CS has been extensitvely reported as a biocompatible polysaccharide and its is approved in food industry [41]. However, it may elicit cell toxicity *in vitro* when due to a highly positvely-charged surface [36,37,46]. Crosslinking of self-assembled CS-based nanoparticles was implemented to physically stabilize them and to also partly neutralize the net positive surface charge and increase their cell compatibility [30]. This modification was not enough to ensure their good compatibility with human primary nasal epithelium cells [43]. Thus, we produced mixed nanoparticles that reduce the effective CS concentration on the surface and thus, its charge density, while preserving the nanoencapsulation capacity of the nanoparticles and its mucoadhesiveness [43]. Further crosslinking reduced the Z-potential and improved the compatibility of the nanoparticles in primary nasal epithelial cells [43]. We visualized the morphology of non-crosslinked and crosslinked nanoparticles by high resolution-scanning electron microscopy (HR-SEM). The size was in line with DLS analysis, considering that in HR-SEM the nanoparticles underwent drying as opposed to DLS where the D_h is measured (**Figure 1**). Some aggregation during sample preparation could not be prevented though these aggregates are not present in the nanoparticle suspension.
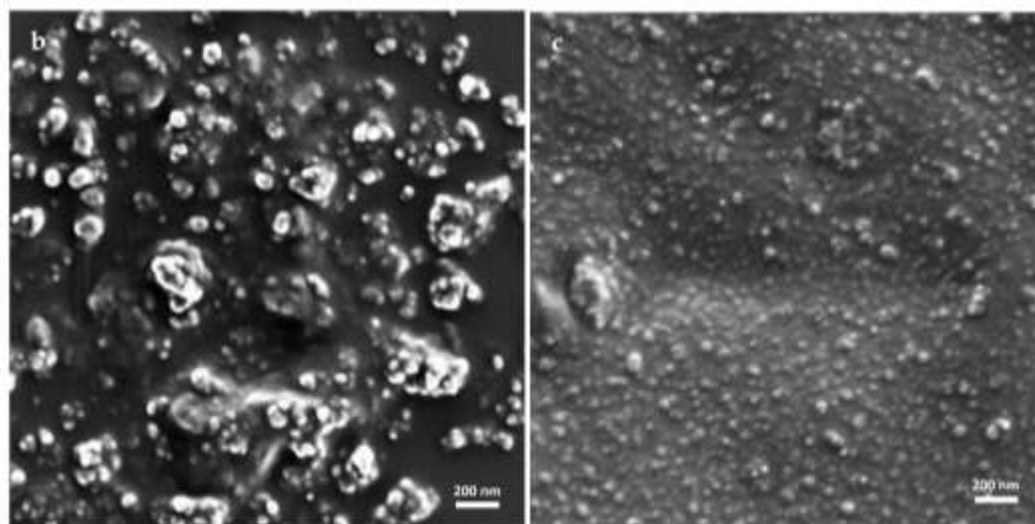
Figure 1. HR-SEM micrographs of mixed CS-*g*-PMMA:PVA-*g*-PMMA nanoparticles. (a) non-crosslinked and (b) crosslinked nanoparticles.

In a previous work, we showed that these nanoparticles cross a model of the human nasal epithelium *in vitro* [43], and hypothesized that they could effectively reach the CNS upon i.n. administration. In this framework, the main goal of this work was to investigate for the first time the biodistribution and accumulation in the brain and other organs of mixed CS-PMMA30:PVA-PMMA16 nanoparticles after i.n. administration to Hsd:ICR mice and compare it to the i.v. route. Since crosslinked nanoparticles are physically stable, as opposed to the non-crosslinked counterparts, for this preliminary study, 0.1% w/v crosslinked mixed CS-PMMA30:PVA-PMMA16 nanoparticles were labeled with the near infrared (NIR) dye NIR-797 and 200 μL of the nanoparticle suspension was injected i.v. through the tail vein (total nanoparticle dose of 8 mg/kg) or 20 μL of the same formulation was administered i.n. (total nanoparticle dose of 0.8 mg/kg). It is important to highlight that in this preliminary study, the nanoparticle dose administered i.n. was 10-fold smaller than i.v. At predetermined time points, live animal screening was performed using IVIS Spectrum In Vivo Imaging System. After i.v. administration, nanoparticles reach the systemic circulation and interact with the reticuloendothelial system, a system of macrophages mostly in the liver that could sequester the nanoparticles due the recognition of opsonins (serum proteins), while nanoparticles with size of up to 5-10 nm could undergo renal filtration [47]. At different time points post-administration (0-24 h), mice were sacrificed, the different organs carefully dissected and the average fluorescence radiance (AFR) of each organ was quantified by subtracting the basal signal of each organ in control (untreated) animals (**Figure 2**). After i.v. administration, the highest accumulation at the different time points was observed in the liver (**Figure 2a**), as described for other nanoparticles of similar size and composition upon i.v. administration [48-50]. Other organs showed lower AFR associated with a more limited nanoparticle accumulation. According to the size (several hundreds of nanometers), these nanoparticles do not undergo renal filtration. Thus, their detection in the kidneys is most probably related to their accumulation in the renal tissue (e.g., proximal tube epithelium) [51].

Intranasal is a local administration route that capitalizes on the nose-to-brain transport to surpass the BBB and target different parts of the brain. Thus, accumulation in peripheral organs such as the liver was expected to take place a very limited extent [52]. After i.n. administration, the accumulation of the nanoparticles in off-target organs was much lower than after i.v. injection (**Figure 2b**). Moreover, a comparison of the AFR values in the different organs at different time points (0-4 h) after i.n. and i.v. administration revealed that some of the differences between both administration routes are statistically significant (**Supplementary Table 2**). In particular, the accumulation of the nanoparticles in the liver, which is the main clearance organ for nanoparticulate matter in this size range, after i.n. administration was up to 20 times lower than by i.v. even that the dose was 10 times

smaller; intranasally administered nanoparticles could reach peripheral organs after redistribution from the CNS to the systemic circulation [53,54]. These results highlight the benefit of i.n. administration to reduce off-target delivery and toxicity.
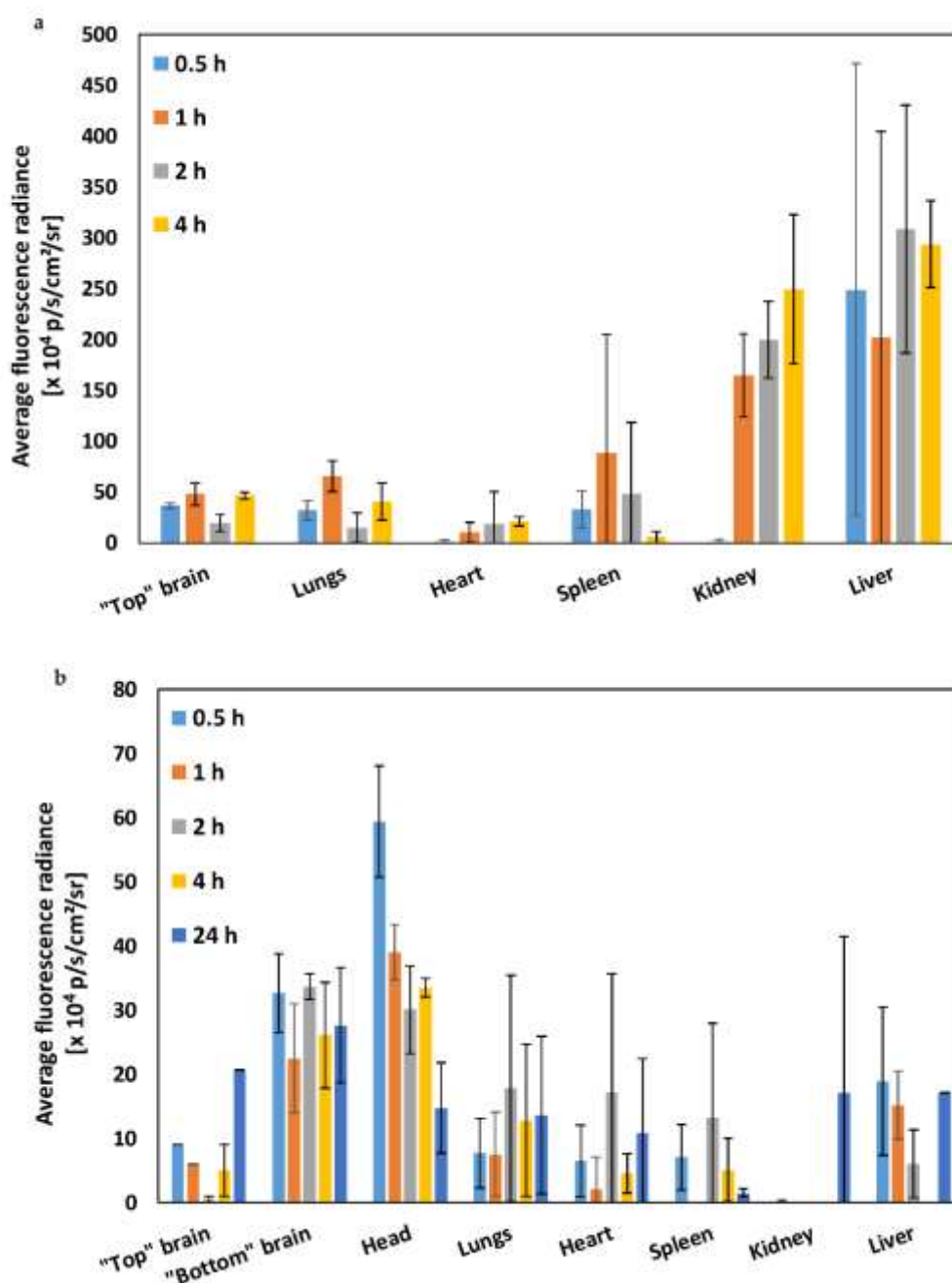
Figure 2. Biodistribution of NIR-797-labelled crosslinked 0.1% w/v mixed CS-PMMA30:PVA-PMMA16 nanoparticles after (a) i.v. administration and (b) i.n. administration to Hsd:ICR mice (n = 3). The measurement was performed after organ dissection at each time point. Average fluorescence radiance was measured using Living Imaging analysis software. Bars represent the average of mice at each time point. The error bars are S.D. from the mean. Statistical comparisons are summarized in Supplementary Table 2.

The imaging system used in this study normalizes the AFR to the organ that displays the maximum intensity, in this case the liver. Thus, we imaged the brains separately from the other organs (in triplicates) at different time points (0-24 h, depending on the administration route) and estimated the

nanoparticle accumulation in the "top" brain (i.v. and i.n. administration), and "bottom" brain and head (i.n. administration) (**Figure 3a**). Upon i.v. administration (0-4 h), our nanoparticles accumulated mainly in the "top" brain. Later time points were not investigated in this preliminary study because we previously showed the relatively limited bioavailability of this type of nanoparticle in the CNS of mouse after i.v. administration and the need for the surface modification with ligands that bind receptors expressed on the apical side of the BBB endothelium [50]. We were more interested in exploring the behavior of intranasally administered nanoparticles and thus, we tracked them for 24 h. Different i.n. administration methods and formulations could affect the biodistribution of the drug-loaded nanoparticles in the CNS and the pharmacological outcome. For example, Martins *et al*. showed that the i.n. administration of oxytocin with a nebulizer leads to a different pharmacological outcome compared to a standard nasal spray [55]. These results highlight the complexity of this transport pathway and the difficulty of comparing among different works. After i.n. administration, particles are expected to enter the CNS through the olfactory region and accumulate in the nose, the nose-to-brain track (e.g., olfactory bulb) and the "bottom" brain (**Figure 3a**), before they disseminate to all the brain [21,56].
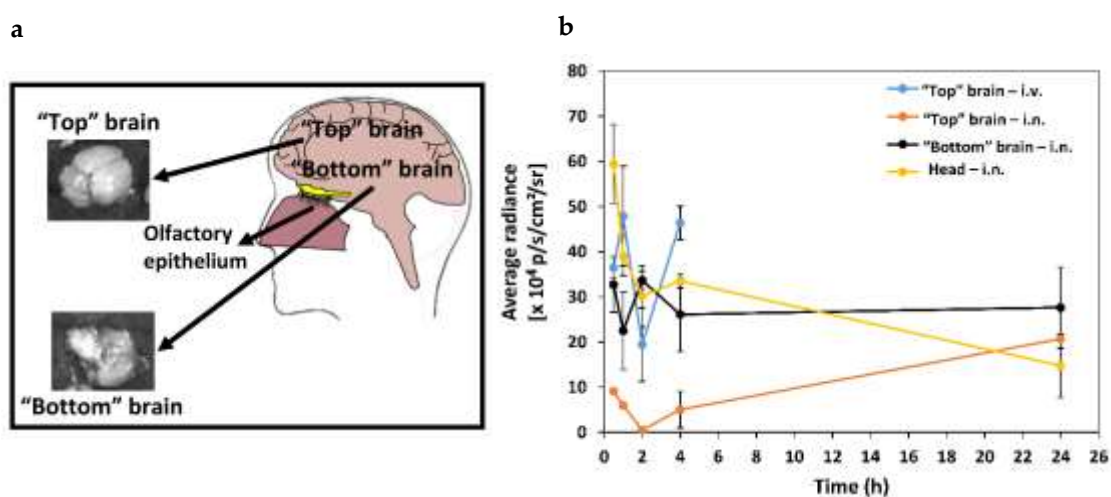
Figure 3. *Ex vivo* analysis of the distribution of NIR-797-labeled crosslinked 0.1% w/v mixed CS-PMMA30:PVA-PMMA16 nanoparticles in the brain following i.v. and i.n. administration to Hsd:ICR mice (n = 3). (a) Scheme of the top and bottom brain and (b) average radiance over time obtained after the subtraction of the control (untreated mice brain) radiance (n = 3).

The highest AFR value was measured in the "top" brain 1 h after i.v. injection (**Figure 3b**). At this point, we analyzed the bottom side of the brain after i.n. administration because after penetrating through the olfactory epithelium, the nanoparticles could be accumulated in this area of the CNS close to the pons and serve as a reservoir from which an encapsulated drug could be released. Two hours after i.n. administration, the accumulation in the "bottom" brain was significantly higher than upon i.v. injection. We further calculated the AFR in the brain (with subtraction of the control signal) at each time point and compared values of area under the curve (AUC) between 0 and 4 h ($AUC_{0-4 h}$). Nanoparticle accumulation in the "bottom" brain after i.n. administration ($AUC_{0-4 h} = 110 \pm 10 \times 10^{4}$ p/s/cm²/sr) was similar and not significantly different from that of intravenously administered nanoparticles in the "top" brain ($AUC_{0-4 h} = 130 \pm 20 \times 10^{4}$ p/s/cm²/sr) (**Figure 3b, Table 1**). These results indicate that a similar brain bioavailability could be reached with a 10 times smaller dose. At the same time, it is important to point out that in the case of i.n. administration, these mucoadhesive nanoparticles could be initially retained in the nasal mucosa and accumulate in the nose-to-brain track and, at a later stage, be released and diffuse across the brain tissue to reach more distant areas.

In general, two beneficial phenomena are observed after i.n. administration when compared to i.v.: (i) there is higher accumulation in the brain [52] and (ii) the accumulation is less spread, enabling targeting of the nanoparticles to more specific CNS regions, which is associated with the nanoparticle properties [57] and probably to the type of nasal nanoformulation [55]. After i.n. administration, our mucoadhesive nanoparticles reached the brain fast (less than 1 h) and could be detected mainly in the head due to their retention in the nose and accumulated mainly in the "bottom" brain, while the AFR in the "top" one was relatively low. The fast delivery of nanoparticles to the brain upon i.n. administration has been reported in the literature [58,59]. It is also important to stress that nose tissues were not isolated and thus, the whole head without the brain was imaged to estimate the retention of the nanoparticles in the nasal mucosa. The $AUC_{0-4 h}$ in the "bottom" brain was significantly higher than that in the "top" brain, indicating that the nanoparticles initially accumulate in the nose-brain tract (**Figure 3b**, **Table 1**). At 24 h, the AFR in the "bottom" brain remained almost constant (AFR ratio between 24 and 4 h was 1.06) and it increased by 4-fold in the "top" brain with respect to 4 h, at the expense of the AFR detected in the head/nose. A similar trend was followed by the $AUC_{0-24 h}$ that showed a moderate increase in the "bottom" brain from 110 ± 18 to 164 ± 7 $AUC_{0-24 h}$ (x 10^4 p/s/cm²/sr) and a more pronounced one in the "top" brain from 15 ± 4 to 41 ± 3 $AUC_{0-24 h}$ (x 10^4 p/s/cm²/sr) (**Table 1**). These findings suggest that the nanoparticles are transported from the nasal mucosa and the "bottom" brain to other brain areas at a slower rate, leading to these changes in the $AUC_{0-24 h}$ values. Most previous research utilizing i.n. delivery of nanomedicines disregarded the possible differential biodistribution and assumed that all the brain areas are exposed to similar nanoparticle concentrations. Our results with mixed CS-PMMA30:PVA-PMMA16 nanoparticles demonstrate that they are not homogeneously distributed in the brain soon after administration. In addition, they strongly suggest that with the proper nanoparticle design, specific structures of the CNS could be targeted to treat different medical conditions affecting them.

Table 1. Average fluorescence radiance obtained from different brain regions and the head after the subtraction of the control (untreated mice) radiance at different time points and calculated $AUC_{0-4 h}$ values.

Brain region	$AUC_{0-4 h}$ (x 10^4 p/s/cm²/sr) ± S.D.	$AUC_{0-24 h}$ (x 10^4 p/s/cm²/sr) ± S.D.
"Top" brain – i.v.	130 ± 20*	N.D.
"Top" brain – i.n.	15 ± 4	41 ± 3*****
"Bottom" brain – i.n.	110 ± 18**	164 ± 7**,,****,*****
Head – i.n.	138 ± 17***	186 ± 6*****

N.D.: Not determined. *Statistically significant difference between $AUC_{0-4 h}$ in the "top" brains of mouse after i.v. and i.n. administration (P <0.05); **statistically significant $AUC_{0-4 h}$ and $AUC_{0-24 h}$ difference between the "top" and "bottom" brains of mouse after i.n. administration (P <0.05); ***statistically significant $AUC_{0-4 h}$ and $AUC_{0-24 h}$ difference between the "top" brain and the head of mouse after i.n. administration (P <0.05); ****statistically significant $AUC_{0-24 h}$ difference between the "bottom" brain and the head of mouse after i.n. administration (P <0.05); *****statistically significant differences between $AUC_{0-24 h}$ and $AUC_{0-4 h}$ after i.n. administration (P <0.05).

Having said this, more studies need to be conducted to realize this potential. Future studies will investigate the pharmacokinetics of encapsulated drugs in the CNS upon i.v. and i.n. administration and will also include later time points.

3. Methods

3.1. Synthesis of the chitosan-g-poly(methyl methacrylate) and poly(vinyl alcohol)-g-poly(methyl methacrylate) copolymers

A CS-*g*-PMMA copolymer containing 30% w/w of PMMA (CS-PMMA30, as determined by proton-nuclear magnetic resonance [29,30]), was synthesized by the graft free radical polymerization of MMA (99% purity, Alfa Aesar, Heysham, UK) onto the CS backbone in water. For this, low molecular weight CS (0.4 g, degree of deacetylation of 94%; viscosity ≤ 100 mPa.s, Glentham Life Sciences, Corsham, UK) was dissolved in nitric acid 70% (0.05 M in water, 100 mL) that was degassed by sonication (30 min, Elmasonic S 30, Elma Schmidbauer GmbH, Singen, Germany). Then, a tetramethylethylenediamine (TEMED, Alfa Aesar) solution (0.18 mL in 50 mL of degassed water) was poured into the CS solution and purged with nitrogen for 30 min at RT. The purged CS solution was magnetically stirred and heated to 35°C and 142 µL of MMA (distilled under vacuum to remove inhibitors before use) was added to the degassed water (48 mL) and then mixed with the CS solution. Finally, a cerium (IV) ammonium nitrate (CAN, Strem Chemicals, Inc., Newburyport, MA) solution (0.66 g in 2 mL of degassed water) was added to the polymerization reaction that was allowed to proceed for 3 h at 35°C and under continuous nitrogen flow. After 3 h, the polymerization was quenched by adding 0.13 g of hydroquinone (Merck, Hohenbrunn, Germany). The product was purified by dialysis against distilled water using a regenerated cellulose dialysis membrane with molecular weight-cut off (MWCO) of 12–14 kDa (Spectra/Por® 4 nominal flat width of 75 mm, diameter of 48 mm and volume/length ratio of 18 mL/cm, Spectrum Laboratories, Inc., Rancho Dominguez, CA, USA) for at 48–72 h and freeze-dried. The same chemical pathway with small modifications was used to synthesize a PVA-*g*-PMMA copolymer containing 16% w/w of PMMA (PVA-PMMA16) [31]. First, PVA (0.4 g) was dissolved in distilled water (100 mL) at RT and TEMED (0.18 mL in 50 mL of degassed water) was dissolved in nitric acid 70% (0.45 mL). Then, TEMED and PVA solutions were degassed by sonication for 30 min, mixed and purged with nitrogen for 30 min at RT. The solution was heated to 35°C and 142 µL of MMA dispersed in degassed water (48 mL) and added to the reaction mixture. Finally, a CAN solution (0.66 g in 2 mL of degassed water) was added and the reaction allowed to proceed for 2 h at 35°C. The reaction product was purified by dialysis and freeze-dried. Products were stored at 4°C until use.

For biodistribution studies (see below), CS-PMMA30 and PVA-PMMA16 copolymers were fluorescently-labeled with the near infrared tracer NIR-797 isothiocyanate (Sigma-Aldrich, St. Louis, MO, USA). For this, CS-PMMA30 (80 mg) was dissolved in 8 mL water supplemented with acetic acid (pH = 5.5), prepared by diluting 70 µL of glacial acetic acid (Bio-Lab Ltd., Jerusalem, Israel) in 1 L of water under magnetic stirring. Then, NIR-797 (0.4 mg) was dissolved in *N,N*-dimethylformamide (0.2 mL, DMF, Bio-Lab Ltd.), added to the copolymer solution and the mixture stirred for 16 h protected from light, at RT. Finally, the product was dialyzed (48 h, regenerated cellulose dialysis membrane, MWCO of 3500 Da, Membrane Filtration Products, Inc., Seguin, TX, USA), freeze-dried (72–96 h) and stored protected from light at 4°C until use. In the case of PVA-PMMA16, the copolymer (100 mg) was dissolved in 3 mL DMF under magnetic stirring. Then, NIR-797 (0.8 mg) was dissolved in DMF (0.1 mL), added to the copolymer solution and the mixture stirred for 16 h protected from light, at RT. The reaction mixture was diluted with deionized water (1:2 v/v), dialyzed (48 h, regenerated cellulose dialysis membrane, MWCO of 3500 Da) to remove unreacted NIR-797, freeze-dried (72–96 h) and stored protected from light at 4°C until use. The theoretical NIR-797 content was between 0.5-0.8% w/w.

3.2. Preparation and characterization of mixed chitosan-g-poly(methyl methacrylate):poly(vinyl alcohol)-g-poly(methyl methacrylate) nanoparticles

Identical amounts of CS-PMMA30 and PVA-PMMA16 were dissolved in dimehtyl sulfoxide (DMSO) to reach a total copolymer concentration of 0.5% w/v under continuous stirring (24 h), at 37°C. Subsequently, the solution was dried under vacuum utilizing a freeze-dryer, the copolymer

mixture re-dispersed in water supplemented with acetic acid (pH = 5.5) to reach a final total copolymer concentration of 0.1% w/v and filtered (1.2 μm cellulose acetate syringe filter, Sartorius Stedim Biotech GmbH, Göttingen, Germany). For physical stabilization, 0.1% w/v nanoparticles were crosslinked by the addition of 1% w/v TPP (Sigma-Aldrich) aqueous solution (2.5 μL of crosslinking solution per mL of 0.1% w/v nanoparticle dispersion).

The size (expressed as hydrodynamic diameter, D_h), size distribution (PDI) and the Z-potential (an estimation of the surface charge density) of 0.1% w/v systems were measured using the Zetasizer Nano-ZS in the same media detailed above for the different samples. Z-potential measurements of the same samples required the use of laser Doppler micro-electrophoresis in the Zetasizer Nano-ZS. Each value obtained is expressed as mean ± standard deviation (S.D.) of at least three independent samples, while each DLS or Z-potential measurement is an average of at least seven runs.

The morphology of mixed nanoparticles before and after crosslinking was visualized by HR-SEM (carbon coating, acceleration voltage of 2-4 kV, Ultraplus, Zeiss, Oberkochen, Germany). For this, mixed nanoparticle suspensions (0.5% w/v total copolymer concentration), drop-casted on silicon wafer, dried at 37 °C in the oven and carbon-coated. Images were obtained using In-lens detector at 3-4 mm working distance. The nanosuspensions were sprayed on top of a silicon wafer (cz polished silicon wafers <100> oriented, highly doped N/Arsenic, SHE Europe Ltd., Livingston, UK) by introducing high pressure nitrogen which allowed an even spread of the nanoparticles on the wafer. Next, the wafer was attached to the grid using carbon-tape and additional tape was placed on its frame. At the corners of the frame silver paint (SPI# 05002-AB – Silver, SPI supplies, West Chester, PA, USA) was applied and the samples were carbon coated.

3.3. Biodistribution of mixed chitosan-g-poly(methyl methacrylate):poly(vinyl alcohol)-g-poly(methyl methacrylate) nanoparticles

For biodistribution studies, CS-PMMA30 and PVA-PMMA16 copolymers were fluorescently labeled with NIR-797 as described above.

Hsd:ICR mice (Envigo, Jerusalem, Israel) were maintained at the Gutwirth animal facility of the Technion-Israel Institute of Technology. All animal experiments were approved and performed according to the guidelines of the Institutional Animal Research Ethical Committee at the Technion (ethics approval number IL-052-05-18). Animal welfare was monitored daily by the staff veterinarians. Mice fasted for 12 h prior to experiments. Crosslinked mixed CS-PMMA30:PVA-PMMA16 (1:1) nanoparticles (200 μL, 0.1% w/v) were injected i.v. into the tail vein. For i.n. administration, mice were lightly anesthetized with 2.5% isoflurane (USP Terrel™ Piramal Critical Care, Bethlehem, PA, USA), and fixed in a supine position for the administration of 10 μL of the nanoparticles in each nostril using a pipette (total volume of 20 μL, 0.1% w/v). After 0.5, 1, 2, 4 and 24 h post i.v. injection or i.n. administration animals were sacrificed by dislocation and organs (liver, spleen, kidney, lungs, heart, brain and head – nose area) were dissected. Organ screening was performed *ex vivo* using an Imaging System (IVIS, PerkinElmer, Waltham, MA, USA) with an excitation at 795 nm and an emission at 810 nm. Then at the same conditions (see above) image analysis was performed using Living Imaging analysis software (PerkinElmer). The auto fluorescence of organs of the control (untreated) mouse were subtracted. Mice were used in triplicates for each time point. Then, the average radiance in the brain (with subtraction of the control signal) at each time point was calculated, and the values of $AUC_{0\text{-}4\,h}$ determined according to Equation 1 [60]

$$AUC = \sum_i \frac{(t_{i+1} - t_i)}{2 \times (AR_i + AR_{i+1})} \quad (1)$$

Where t_i is the starting time point, t_{i+1} is the finishing time point (0.5, 1, 2 and 4 h), AR_i is the starting value of average fluorescence measured, and AR_{i+1} is the finishing value for each measurement over time.

3.4. Statistical analysis

Statistical analysis of the different experiments was performed by t-test on raw data (Excel, Microsoft Office 2013, Microsoft Corporation). P value smaller than 0.05 were regarded as statistically significant.

Supplementary Materials: The following are available online at www.mdpi.com/xxx/s1
Supplementary Table 1: Hydrodynamic diameter (D_h), size distribution (PDI) and Z-potential of CS-PMMA30, PVA-PMMA16 and CS-PMMA30:PVA-PMMA16 nanoparticles (total copolymer concentration of 0.1% w/v), as determined by DLS. Nanoparticle crosslinking was carried out with 1% w/v TPP.
Supplementary Table 2: Statistical analysis of AFR data in the different organs and time points after i.v. and i.n. administration of mixed CS-PMMA30:PVA-PMMA16 nanoparticles, as analyzed by the IVIS Spectrum In Vivo Imaging System (P <0.05).

Funding: This work was supported by the Israel Science Foundation (ISF, Grant #269/15) and the Teva National Network of Excellence in Neuroscience Research Grant. Partial support of the Russell Berrie Nanotechnology Institute (Technion) is also acknowledged.

Conflicts of Interest: The authors declare no conflict of interest

References

1. Blanco-Prieto, M. Drug Delivery to the Central Nervous System: A Review. *J. Pharm. Sci.* **2003**, *6*, 252–273.
2. Pardridge, W. Non-Invasive Drug Delivery to the Human Brain Using Endogenous Blood-Brain Barrier Transport Systems. *Pharm. Sci. Technol. Today.* **1999**, *2*, 49–59.
3. Oller-Salvia, B.; Sanchez-Navarro, M.; Giralt, E.; Teixido, M. Blood-Brain Barrier Shuttle Peptides: An Emerging Paradigm for Brain Delivery. *Chem. Soc. Rev.* **2016**, *45* (17), 4690–4707.
4. Löscher, W., Potschka, H. Blood-Brain Barrier Active Efflux Transporters: ATP-Binding Cassette Gene Family. *NeuroRx* **2005**, *2*, 86–98.
5. Dallas, S.; Miller, D.S.; Bendayan, R. Multidrug Resistance-Associated Proteins: Expression and Function in the Central Nervous System. *Pharmacol. Rev.* **2006**, *58*, 140–161.
6. Zeiadeh, I.; Najjar, A.; Karaman, R. Strategies for Enhancing the Permeation of CNS-Active Drugs through the Blood-Brain Barrier: A Review. *Molecules* **2018**, *23*, 1289.
7. Rapoport, S.I. Osmotic Opening of the Blood–Brain Barrier: Principles, Mechanism, and Therapeutic Applications. *Cell Mol. Neurobiol.* **2000**, *20*, 217–230.
8. Ohtsuki, S., Terasaki, T. Contribution of Carrier-Mediated Transport Systems to the Blood–Brain Barrier as a Supporting and Protecting Interface for the Brain; Importance for CNS Drug Discovery and Development. *Pharm. Res.* **2007**, *24*, 1745–1758.
9. Tsuji, A. Small Molecular Drug Transfer Across the Blood-Brain Barrier via Carrier-Mediated Transport Systems. *NeuroRx* **2005**, *2*, 54–62.
10. Gomes M.J., Mendes B., Martins S., Sarmento B. (2016) Nanoparticle Functionalization for Brain Targeting Drug Delivery and Diagnostic. In: Aliofkhazraei M. (eds) Handbook of Nanoparticles. Springer, Cham.
11. Gabathuler, R. Approaches to Transport Therapeutic Drugs Across the Blood-Brain Barrier to Treat Brain Diseases. *Neurobiol. Dis.* **2010**, *37*, 48–57.
12. Fang, F.; Zou, D.; Wang, W.; Yin, Y.; Yin, T.; Hao, S.; Wang, B.; Wang, G.; Wang, Y. Non-Invasive Approaches for Drug Delivery to the Brain Based on the Receptor Mediated Transport. *Mater. Sci. Eng. C* **2017**, *76*, 1316–1327.
13. Tam, V.H.; Sosa, C.; Liu, R.; Yao, N.; Priestley, R.D.; Nanomedicine as a Non-Invasive Strategy for Drug Delivery Across the Blood Brain Barrier. *Int. J. Pharm.* **2016**, *515*, 331–342.
14. Gaillard, P.J.; Visser, C. C.; Appeldoorn, C.C.M.; Rip, J. Enhanced Brain Drug Delivery: Safely Crossing the Blood-Brain Barrier. *Drug Discov. Today Technol.* **2012**, *9*, 155–160.
15. Wong, H.L.; Wu, X.Y.; Bendayan, R. Nanotechnological Advances for the Delivery of CNS Therapeutics. *Adv. Drug Deliv. Rev.* **2012**, *64*, 686–700.

16. Saraiva, C.; Praca, C.; Ferreira, R.; Santos, T.; Ferreira, L.; Bernardino, L. Nanoparticle-Mediated Brain Drug Delivery: Overcoming Blood-Brain Barrier to Treat Neurodegenerative Diseases. *J. Control. Release.* **2016**, *235*, 34–47.

17. Georgieva, J. V.; Hoekstra, D.; Zuhorn, I. S. Smuggling Drugs into the Brain: An Overview of Ligands Targeting Transcytosis for Drug Delivery across the Blood Brain Barrier. *Pharmaceutics.* **2014**, *6*, 557–583

18. Lucchini, R.G.; Dorman, D.C.; Elder, A.; Veronesi, B. Neurological Impacts from Inhalation of Pollutants and the Nose-Brain Connection. *Neurotoxicology* **2012**, *33*, 838-841.

19. Oberdörster, G.; Sharp, Z.; Atudorei, V.; Elder, A.; Gelein, R.; Kreyling, W.; Cox, C. Translocation of Inhaled Ultrafine Particles to the Brain. *Inhal. Toxicol.* **2004**, *16*, 437-445.

20. Elder, A.; Gelein, R.; Silva, V.; Feikert, T.; Opanashuk, L.; Carter, J.; Potter, R.; Maynard, A.; Ito, Y.; Finkelstein, J.; Oberdörster, G. Translocation of Inhaled Ultrafine Manganese Oxide Particles to the Central Nervous System. *Environ. Health. Perspect.* **2006**, *114*, 1172.

21. Babadjouni, R.; Patel, A.; Liu, Q.; Shkirkova, K.; Lamorie-Foote, K.; Connor, M.; Hodis, D.M.; Cheng, H.; Sioutas, C.; Morgan, T.E.; Finch, C.E.; Mack, W.J. Nanoparticulate Matter Exposure Results in Neuroinflammatory Changes in the Corpus Callosum. *PLOS One* **2018**, *13*, e0206934.

22. Pires, P.C.; Santos, A.O. Nanosystems in Nose-To-Brain Drug Delivery: A Review of Non-Clinical Brain Targeting Studies. *J. Control. Release* **2018**, *270*, 89-100.

23. Feng, Y.; He, H.; Li, F.; Lu, Y.; Qi, J.; Wu, W. An Update on the Role of Nanovehicles in Nose-to-Brain Drug Delivery. *Drug Discov. Today* **2018**, *23*, 1079-1088.

24. Hanson, L.R.; Frey, W.H. Intranasal Delivery Bypasses the Blood-Brain Barrier to Target Therapeutic Agents to the Central Nervous System and Treat Neurodegenerative Disease. *BMC Neurosci.* **2008**, *9*, S5.

25. Perez, A.P.; Mundiña-Weilenmann, C.; Romero, E.L.; Morilla, M.J. Increased Brain Radioactivity by Intranasal P-labeled siRNA Dendriplexes Within in Situ-Forming Mucoadhesive Gels. *Int. J. Nanomedicine* **2012**, *7*, 1373-1385.

26. Kumar, A.; Pandey, A.N.; Jain, S.K. Nasal-Nanotechnology: Revolution for Efficient Therapeutics Delivery. *Drug Deliv.* **2016**, *23*, 671-683.

27. Pires, P. C.; Santos, A. O. Nanosystems in Nose-to-Brain Drug Delivery: A Review of Non-Clinical Brain Targeting Studies. *J. Control. Release* **2018**, *270*, 89–100.

28. Chiappetta, D.A.; Hocht, C.; Opezzo, J.A.W.; Sosnik, A, Intranasal Administration of Antiretroviral-Loaded Micelles for Anatomical Targeting to the Brain in HIV. *Nanomedicine (Lond.)* **2013**, *8*, 223-237.

29. Kanazawa, T.; Taki, H.; Tanaka, K.; Takashima, Y.; Okada, H. Cell-Penetrating Peptide-Modified Block Copolymer Micelles Promote Direct Brain Delivery via Intranasal Administration. *Pharm. Res.* **2011**, *28* (9), 2130–2139.

30. Raskin Menaker, M.; Schlachet, I.; Sosnik, A. Mucoadhesive Nanogels by Ionotropic Crosslinking of Chitosan-*g*-Oligo(NiPAam) Polymeric Micelles as Novel Drug Nanocarriers. *Nanomedicine (Lond.).* **2016**, *11*, 217–233.

31. Moshe, H.; Davizon, Y.; Menaker Raskin, M.; Sosnik, A. Novel Poly(Vinyl Alcohol)-Based Amphiphilic Nanogels by Boric Acid Non-Covalent Crosslinking of Polymeric Micelles. *Biomater. Sci.* **2017**, *5*, 2295-2309.

32. Noi, I.; Schlachet, I.; Kumarasamy, M.; Sosnik, A. Permeability of Chitosan-*g*-Poly(Methyl Methacrylate) Amphiphilic Nanoparticles in a Model of Small Intestine *In Vitro*. *Polymers* **2018**, *10*, 478.

33. Schlachet, I.; Trousil, J.; Rak, D.; Knudsen, K.D.; Pavlova, E.; Nyström, B.; Sosnik, A. Chitosan-*graft*-Poly(Methyl Methacrylate) Amphiphilic Nanoparticles: Self-Association and Physicochemical Characterization. *Carbohydr. Polym.* **2019**, *212*, 412-420.

34. Moshe Halamish, H.; Trousil, J.; Rak, D.; Knudsen, K.D.; Pavlova, E.; Nyström, B.; Štěpánek, P.; Sosnik, A. Self-Assembly and Nanostructure of Poly(Vinyl Alcohol)-*graft*-Poly(Methyl Methacrylate) Amphiphilic Nanoparticles. *J. Colloid Interface Sci.* **2019**, *553*, 512-523.

35. Kumarasamy, M.; Sosnik, A. The Nose-to-Brain Transport of Polymeric Nanoparticles is Mediated by Immune Sentinels and Not by Olfactory Sensory Neurons. *Adv. Biosys.* **2019**, *3*, 1900123.

36. Mohammed, M.A.; Syeda, J.T.M.; Wasan, K.M.; Wasan, E.K. An Overview of Chitosan Nanoparticles and Its Application in Non-Parenteral Drug Delivery. *Pharmaceutics* **2017**, *9*, 53.

37. Ways, M.; Lau, W.M., Khutoryanskiy, V.V. Chitosan and Its Derivatives for Application in Mucoadhesive Drug Delivery Systems. *Polymers* **2018**, *10*, 267.

38. Alam, S.; Khan, Z. I.; Mustafa, G.; Kumar, M.; Islam, F.; Bhatnagar, A.; Ahmad, F. J. Development and Evaluation of Thymoquinone-Encapsulated Chitosan Nanoparticles for Nose-to-Brain Targeting: A Pharmacoscintigraphic Study. *Int. J. Nanomedicine* **2012**, *7*, 5705–5718.

39. Casettari, L; Illum, L. Chitosan in Nasal Delivery Systems for Therapeutic Drugs. *J. Control. Release* **2014**, *190*, 189-200.

40. Rassu, G; Soddu, E.; Cossu, M.; Gavini, E.; Giunchedi, P.; Dalpiaz, A. Particulate Formulations Based on Chitosan for Nose-to-Brain Delivery of Drugs. A Review. *J. Drug Deliv. Sci. Technol.* **2016**, *32*, 77–87.

41. Marques C., Som C., Schmutz M., Borges O., Borchard G. How the Lack of Chitosan Characterization Precludes Implementation of the Safe-by-Design Concept. *Front. Bioeng. Biotechnol.* **2020**, 8, 165.

42. Hu, Y.-L.; Qi, W.; Han, F.; Shao, J.-Z.; Gao, J.-Q. Toxicity Evaluation of Biodegradable Chitosan Nanoparticles Using a Zebrafish Embryo Model. *Int. J. Nanomedicine* **2011**, 6, 3351-3359.

43. Schlachet, I.; Sosnik, A. Mixed Mucoadhesive Amphiphilic Polymeric Nanoparticles Cross a Model of Nasal Septum Epithelium In Vitro. *ACS Appl. Mater. Interfaces* **2019**, *11*, 21360–21371.

44. Schlachet, I. Innovative Nano-Biomaterials for the Improved delivery of Antitumorals to the Central Nervous System in the Therapy of Pediatric Brain Tumors, Ph.D. Thesis, Technion-Israel Institute of Technology, **2019**.

45. Gaucher, G.; Dufresne, M.-H.; Sant, V. P.; Kang, N.; Maysinger, D.; Leroux, J.-C. Block Copolymer Micelles: Preparation, Characterization and Application in Drug Delivery. *J. Control. Release.* **2005**, *109*, 169–188.

46. Fröhlich, E. The Role of Surface Charge in Cellular Uptake and Cytotoxicity of Medical Nanoparticles. *Int. J. Nanomedicine* **2012**, *7*, 5577–5591.

47. Rizeq, B.R.; Younes, N.N.; Rasool, K.; Nasrallah, G.K. Synthesis, Bioapplications, and Toxicity Evaluation of Chitosan-Based Nanoparticles. *Int. J. Mol. Sci.* **2019**, *20*, 5776.

48. Ernsting, M. J.; Murakami, M.; Roy, A.; Li, S. D. Factors Controlling the Pharmacokinetics, Biodistribution and Intratumoral Penetration of Nanoparticles. *J. Control. Release* **2013**, *172*, 782–794.

49. He, C.; Hu, Y.; Yin, L.; Tang, C.; Yin, C. Effects of Particle Size and Surface Charge on Cellular Uptake and Biodistribution of Polymeric Nanoparticles. *Biomaterials* **2010**, *31*, 3657–3666.

50. Bukchin, A.; Sanchez-Navarro, M.; Carrera, A.; Teixidó, M.; Carcaboso, A.M.; Giralt, E.; Sosnik, A. Amphiphilic Polymeric Nanoparticles Modified with a Retro-Enantio Peptide Shuttle Target the Brain of Mice, Chem Mater, in press, **2020**. DOI: 10.1021/acs.chemmater.0c01696

51. Williams, R.M.; Shah, J.; Ng, B.D.; Minton, D.R.; Gudas, L.J.; Park, C.Y.; Heller, D.A. Mesoscale Nanoparticles Selectively Target the Renal Proximal Tubule Epithelium. *Nano Letters* **2015**, 15, 2358–2364.

52. Yadav, S.; Gattacceca, F.; Panicucci, R.; Amiji, M. M. Comparative Biodistribution and Pharmacokinetic Analysis of Cyclosporine-A in the Brain upon Intranasal or Intravenous Administration in an Oil-in-Water Nanoemulsion Formulation. *Mol. Pharmaceutics* **2015**, *12*, 1523–1533.

53. Gao, X.; Chen, J.; Chen J.; Wu, B.; Chen, H.; Jiang, X. Quantum Dots Bearing Lectin-Functionalized Nanoparticles as a Platform for In Vivo Brain Imaging. *Bioconjug. Chem.* **2008**, *19*, 2189-2195.

54. Sekerdag. E.; Lüle, S.; Bozdağ Pehlivan, S.; Öztürk, N.; Kara, A.; Kaffashi, A.; Vural, I.; Işıkay, I.; Yavuz, B.; Oguz, K.K.; Söylemezoğlu, F.; Gürsoy-Özdemir, Y.; Mut, M. A Potential Non-Invasive Glioblastoma Treatment: Nose-to-Brain Delivery of Farnesylthiosalicylic Acid Incorporated Hybrid Nanoparticles. *J. Control. Release* **2017**, 261, 187-198.

55. Martins, D.A.; Mazibuko, N.; Zelaya, F.; Vasilakopoulou, S.; Loveridge, J.; Oates, A.; Maltezos, S.; Mehta, M.; Wastling, S.; Howard, M.; McAlonan, G.; Murphy, D.; Williams, S.C.R.; Fotopoulou, A.; Schuschnig, U.; Paloyelis, Y. Effects of Route of Administration on Oxytocin-Induced Changes in Regional Cerebral Blood Flow in Humans. *Nat. Commun.* **2020**, 11, 1160.

56. Shiga, H.; Taki, J.; Yamada, M.; Washiyama, K.; Amano, R.; Matsuura, Y.; Matsui, O.; Tatsutomi, S.; Yagi, S.; Tsuchida, A.; Yoshizaki, T.; Furukawa, M.; Kinuya, S.; Miwa, T. Evaluation of the Olfactory Nerve Transport Function by SPECT-MRI Fusion Image with Nasal Thallium-201 Administration. *Mol. Imaging Biol.* **2011**, *13*, 1262-1266.

57. McGowan, J.W.D.; Shao, Q.; Vig, P.J.S.; Bidwell, G.L. Intranasal Administration of Elastin-like Polypeptide for Therapeutic Delivery to the Central Nervous System. *Drug Des. Devel. Ther.* **2016**, 10, 2803–2813.

58. Xia, H.; Gao, X.; Gu, G.; Liu, Z.; Zeng, N.; Hu, Q.; Song, Q.; Yao, L.; Pang, Z.; Jiang, X.; Chen, J.; Chen, H. Low molecular weight protamine-functionalized naoparticles for drug delivery to the brain after intranasal administration. *Biomaterials* **2011**, 32, 9888-9898.

59. Md, S.; Khan, RA.; Mustafa, G.; Chuttani, K.; Baboota, S.; Sahni, JK.; Ali J. Bromocriptine loaded chitosan nanoparticles intended for direct nose to brain delivery: pharmacodynamic, pharmacokinetic and scintigraphy study in mice model. *Eur. J. Pharm. Sci.* **2013**, 48, 393-405.

60. Pardi, N.; Hogan, M. J.; Naradikian, M. S.; Parkhouse, K.; Cain, D. W.; Jones, L.; Moody, M. A.; Verkerke, H. P.; Myles, A.; Willis, E.; LaBranche, C.C.; Montefiori, D.C.; Lobby, J.L.; Saunders, K.O.; Liao, H.X.; Korber, B.T.; Sutherland, L.L.; Scearce, R.M.; Hraber, P.T.; Tombácz, I.; Muramatsu, H.; Ni, H.; Balikov, D.A.; Li, C.; Mui, B.L.; Tam, Y.K.; Krammer, F.; Karikó, K.; Polacino, P.; Eisenlohr, L.C.; Madden, T.D.; Hope, M.J.; Lewis, M.G.; Lee, K.K.; Hu, S.L.; Hensley, S.E.; Cancro, M.P.; Haynes, B.F.; Weissman, D. Nucleoside-Modified MRNA Vaccines Induce Potent T Follicular Helper and Germinal Center B Cell Responses. *J. Exp. Med.* **2018**, *215*, 1571–1588.